JACS
JOURNAL OF THE AMERICAN CHEMICAL SOCIETY

ARTICLE

pubs.acs.org/JACS

Chromium Porphyrin Arrays As Spintronic Devices

Woo Jong Cho,[†] Yeonchoo Cho,[†] Seung Kyu Min,[†] Woo Youn Kim,[‡] and Kwang S. Kim*[,†]

[†]Department of Chemistry and Department of Physics, Pohang University of Science and Technology, San 31 Pohang, Republic of Korea

[‡]Department of Chemistry, KAIST, Daejeon 305-701, Republic of Korea

Supporting Information

ABSTRACT: Spintronic devices are very important for futuristic information technology. Suitable materials for such devices should have half-metallic properties so that only one spin passes through the device. In particular, organic half metals have the advantage that they may be used for flexible devices and have a long spin-coherence length. We predict that the one-dimensional infinite chromium porphyrin array, which we call Cr−PA$_\infty$, shows half-metallic behavior when the spins on the chromium atoms are in a parallel alignment. Since the chromium atoms are separated by a large distance (>8 Å), the coupling between spins is small and thus their directions can be readily controlled by an external magnetic field. In the ferromagnetic state, the band gap for major spin electrons is 0.30 eV, while there is no band gap for the minor spin electrons, thus reflecting the half-metallic property. This unique property originates from the high spin state of Cr which results in the spin asymmetry of the conduction band in Cr−PA$_\infty$. Electron transport of Cr−PA$_{1,2,3}$ is calculated with the nonequilibrium Green function technique in the presence of Au electrodes. It turned out that the spin-filtering ability appears from the dimeric Cr−PA$_2$. Thus, a new organometallic framework for designing a spin filter is proposed. Though many others have designed novel spintronic devices, none of them are realized due to the lack of a practical fabrication method at present. However, the porphyrin-based spintronic device provides a synthesizable framework.

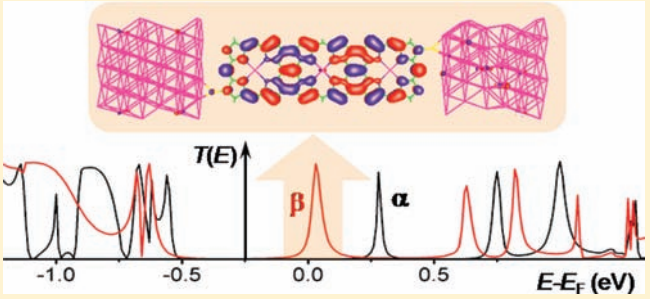

After the emergence of molecular electronics[1−3] which opened new possibilities for the fabrication of electronic devices of ultrahigh density, its spin-polarized version, molecular spintronics soon followed.[4−8] This novel discipline has a wide range of applications from high-capacity storage devices to quantum computers.[9,10] The operation of spintronic devices often requires a pure and coherent spin state, which can be achieved by the use of spin filters.[11,12] However, experimental studies regarding spin filters are difficult. Therefore, theoretical studies should complement experimental ones in order to accelerate the advance of high-performance spintronic devices.

It has been considered that spin filters can be realized by half metals, which are conducting for one spin direction and insulating for the opposite direction.[13,14] Among the various suggested potential half metals, those based on organic molecules deserve special attention due to their long spin coherence length and mechanical flexibility.[15−18] To this end, many such organic/organometallic/inorganic half metals[19−30] have been predicted theoretically. Despite their excellent spin-filtering abilities, their synthetic methods are not feasible or practical. Thus, we hereby suggest another structural framework which may be fabricated by a simple synthetic method, the one-dimensional porphyrin array, for organic spin filters.

Porphyrin derivatives have been known as a good candidate for molecular electronic devices, and their use in molecular

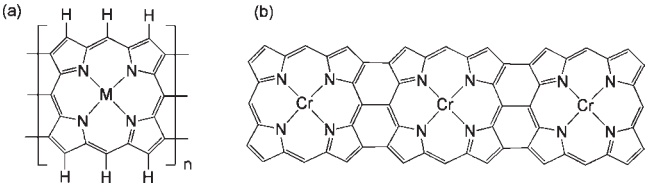

Figure 1. (a) One-dimensional porphyrin array M−PA$_n$, and (b) a representative example Cr−PA$_3$.

electronics has been investigated by both theorists and experimentalists.[31−37] One of the directions is the porphyrin array (PA) composed of n porphyrin rings containing a metal (M) ion in each ring shown in Figure 1 (M−PA$_n$).

Zn−PA$_n$ was experimentally prepared and characterized by Tsuda and Osuka.[38] From the analysis of the UV spectra of several oligomers, they claimed that the porphyrin array can serve as a conducting molecular wire. This conducting property is thought to come from its practically zero band gap. Kang et al. linked both ends of Zn−PA$_n$ to gold electrodes via a Au−S bond and measured the length and temperature dependence of the conductance.[31] However, owing to the closed-shell d[10]

Received: December 23, 2010
Published: May 25, 2011

dx.doi.org/10.1021/ja111565w | J. Am. Chem. Soc. 2011, 133, 9364–9369

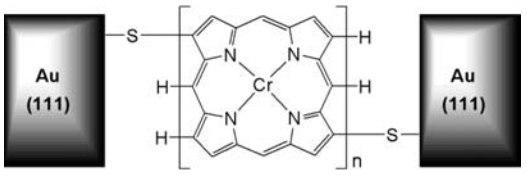

Figure 2. Nanodevice Au−(α,γ)−Cr_n in which Cr−PA_n is linked to two Au(111) electrodes via Au−S bond.

Table 1. Type of Magnetism and Spin-Resolved Occupation Number of the d Orbitals

M		V	Cr	Mn	Fe	Co
$E_{FM} - E_{AFM}$ (eV)		−0.04	0.05	∼0	0.03	0.06
α spin occupation	(calcd)	2.78	3.78	4.07	4.10	4.12
	(model)	3.00	4.00	4.00	4.00	4.00
β spin occupation	(calcd)	0.56	0.44	0.81	2.05	3.07
	(model)	0.00	0.00	1.00	2.00	3.00
excess α spin (calcd)		2.22	3.34	3.26	2.05	1.05

Table 2. Spin-Dependent Band Gaps (eV) of M−PA_∞'s

M	V	Cr	Mn	Fe	Co
major spin	none	0.33	none	none	0.29
minor spin	none	none	none	none	0.20

configuration of the central Zn(II) ion, this porphyrin array cannot be applied to spintronic devices.

We attempt to design a new spintronic device by substituting zinc with other first-row transition metal ions (M = V, Cr, Mn, Fe, and Co) that have a different number of electrons, hence different spin states of the metal. The monomeric M−PA_1's have been synthesized for all the candidate metal ions,[39−42] and Yunqing Chen et al. found that Fe−PA_1 has a considerable spin-polarization in current.[37] Although their oligomers have not been synthesized yet, it is probable that their syntheses will be achieved with a similar methodology used in the synthesis of Zn−PA_n (n > 100).[42] Therefore, it is of importance to investigate their electronic structures and the spin-dependent electron transport.

The band structures of M−PA_∞'s are calculated with density functional theory (DFT). Among the five candidates, Cr−PA_∞ turns out to be the best spintronic device, which will be discussed here. The spin-dependent electron transport of Cr−PA_n (n = 1, 2, 3) in the device Au−(α,γ)−Cr_n (Figure 2) is studied using the nonequilibrium Green function (NEGF) scheme powered by DFT.[43−45] As a result, we find a spin-filtering effect in this device. In order to give a microscopic explanation to this spin-dependent electron transport, electronic structures of the Cr−PA_n dithiols without the gold electrodes are calculated. The spin-dependent electron transport of Cr−PA_n for large n's is qualitatively discussed as well.

Electronic structure calculations of the M−PA_∞'s are performed within the DFT framework using the spin-polarized version of VASP.[46] The exchange-correlation effects are treated within the form of the GGA-PBE functional.[47] The electron−ion interactions are described by the plane-augmented wave (PAW) method.[48] A 99 × 1 × 1 Monkhorst−Pack k points is used, which generated 50 k points in the irreducible region of the first Brillouin zone along the direction of the porphyrin array. In order

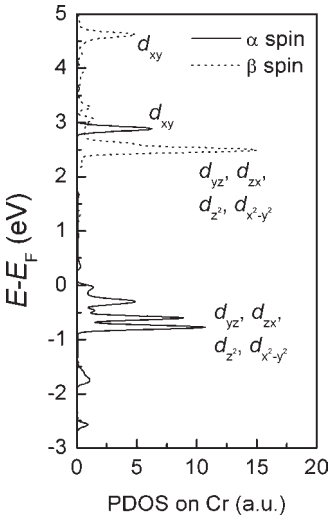

Figure 3. d-orbital contribution to the partial density of states (PDOS) on the chromium atom in Cr−PA_∞. The solid line represents the major spin (α), and the dotted line represents the minor spin (β).

to avoid spurious interactions between images created by the periodicity imposed, we introduce a vacuum region of about 10 Å in the y- and z-axis directions. The cutoff energy is sufficiently high (500 eV) to guarantee accurate results.

The spin-dependent electron transport phenomena of Au−(α,γ)−$Cr_{1,2,3}$ are calculated with the NEGF formalism implemented in POSTRANS,[43,44] which is based on the SIESTA code.[49] The GGA-PBE functional and the single-ζ polarization basis set are used. The transmission functions $T_\sigma(E,V)$ for each spin σ = α, β are calculated at several different bias voltages V. First, the transmission functions of Au−(α,γ)−$Cr_{1,2,3}$ are evaluated at zero bias. Then, transmission functions of Au−(α,γ)−Cr_1 are calculated at finite bias voltages of 0.01, 0.05, and 0.20 V in order to verify that the transmission functions do not change much upon application of a bias voltage. Finally, in order to investigate the nature of conducting orbitals, the electronic structures of Cr−PA_n (n = 2, 3) are computed using the DFT method in the Gaussian 09 package[50] with the B3LYP exchange-correlation and LanL2DZ basis set.

The computational results for the electronic structure of ferromagnetic M−PA_∞'s are summarized in Tables 1 and 2. The ferromagnetic and antiferromagnetic states are almost degenerate in the entire candidate M−PA_∞'s, because the intermetallic distances (∼8.5 Å) are far for the spins to be coupled. Additional noncollinear spin calculations suggest that there is no energy barrier for spin flip, and consequently, the ferromagnetic state can be switched on by means of an external magnetic field when the thermal fluctuation is suppressed at low (∼5 K) temperatures (See Supporting Information). Therefore, these porphyrin arrays under such conditions behave like molecular ferromagnets in the presence of a magnetic field.

The splitting of d orbitals of a transition metal atom surrounded by the porphyrin ligand usually results in four d orbitals close in energy and one high-lying orbital,[51] which we call the '4 + 1 splitting'. In order to explain the magnitude of the magnetic moments listed in Table 1, we hereby employ a simple d-splitting model where there are four degenerate levels and one high-lying level. This model generally agrees with the magnetism calculated with DFT.

dx.doi.org/10.1021/ja111565w |J. Am. Chem. Soc. 2011, 133, 9364–9369

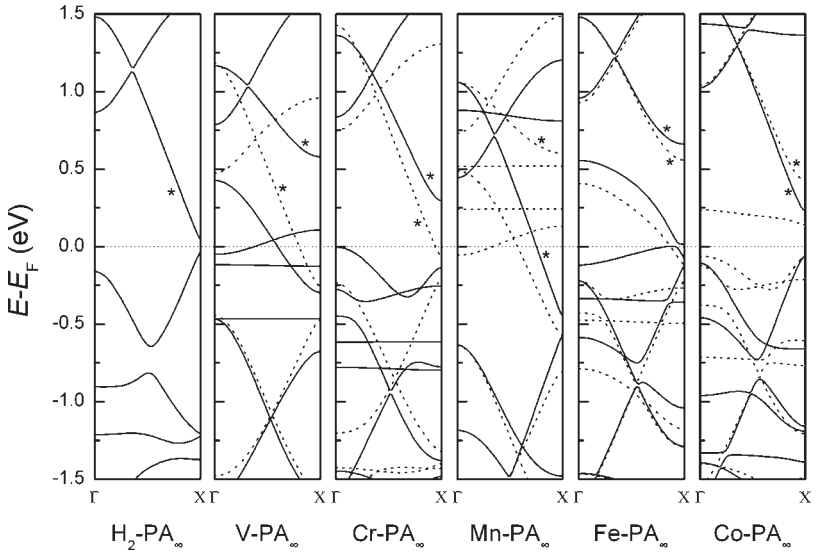

Figure 4. Band structures of M−PA$_\infty$'s for M = H_2, V, Cr, Mn, Fe, and Co. The solid lines represent the major (α) spin, and the dotted lines represent the minor (β) spin. The Fermi level is indicated with a thin dotted line.

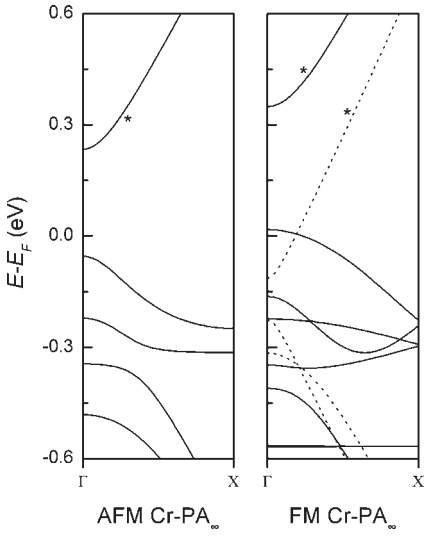

Figure 5. Band structures of antiferromagnetic and ferromagnetic Cr−PA$_\infty$ calculated with a supercell containing two porphyrin units.

As direct evidence to the model, the partial density of states on the chromium atom of Cr−PA$_\infty$ is given in Figure 3. Since the direction of the PA is taken as the *x* axis and the plane on which it lies is regarded as the *xy* plane, the d_{xy} orbital should be the high-lying antibonding σ^* orbital. Although it is unclear in Figure 3, the d_{z^2} and $d_{x^2-y^2}$ orbitals give narrow peaks because they cannot form π bonding due to their symmetries. The d_{xz} and d_{yz} orbitals give broad peaks which arise from the π bonding with the porphyrin moiety.

Deviation from the model decreases as the atomic number increases; thus, V−PA$_\infty$ is the most deviated one. Such behavior may be attributed to the delocalization of α spin density to the adjacent atoms and inflow of β spin density from the adjacent atoms. This delocalization will be less important when the effective nuclear charge is high enough to keep the electrons around the metal ion.

The calculated band structures of M−PA$_\infty$'s are shown in Figure 4, and the band gaps are tabulated in Table 2. It is important to notice in Table 2 that there is a 0.30 eV band gap for the major spin electrons of Cr−PA$_\infty$, whereas the minor spin has none. V−, Mn−, and Fe−PA$_\infty$ form conducting molecular wires since the π bands marked with asterisks allow electron transport. Co−PA$_\infty$ is semiconducting for both spins with a slight difference in the band gaps. Since none of the porphyrin arrays have a band gap difference larger than that of Cr−PA$_\infty$, we confirm that chromium is the best choice for designing a new spin filter. This result remains unchanged even under the DFT+U calculations which are known to give a better description of materials with strong electron correlation.[52,53]

The origin of this spin polarization can be found by comparing the band structures of the PA's with that of the one without central metals. The bands with asterisks in Figure 4 play a key role in the spin-filtering effect. Since the wave function of these bands has the same symmetry as the d_{xz} orbital that has different spin occupation depending on the type of metal atoms, the interaction between them results in different splitting of the asterisked bands for different metal atoms, as shown in Figure 4. Although such a splitting is observed in all the M−PA$_\infty$'s presented, Cr−PA$_\infty$ is the only one with the Fermi energy located within the gap. This positioning of the Fermi level originates from the electron spin configuration in Cr−PA$_\infty$. By the 4 + 1 splitting of d orbitals, minor spin states can be occupied only after filling four major spin states. From the band structures, V−, Mn−, and Fe−PA$_\infty$ are conducting for both electrons because of the partially filled d bands. Co−PA$_\infty$ is semiconducting for both spins because the unoccupied minor spin d band does not mix with the π bands of PA. For the case of Cr−PA$_\infty$, however, the Fermi level intersects d bands of the minor spin, and thus, it is only conducting for the minor spin electrons. It can be explained from the fact that Cr^{2+} is the only one with fully filled low-lying d orbitals for the major spin and empty d orbitals for the minor spin under the 4 + 1 splitting scheme.

Given the small energy difference of ferromagnetic and antiferromagnetic ground states, it is essential to assess the electronic structure of the antiferromagnetic ground state as well. The band structures of both magnetic ground states of Cr−PA$_\infty$ are calculated using a supercell containing two porphyrin units. Those band structures are compared in Figure 5, where it can be seen that

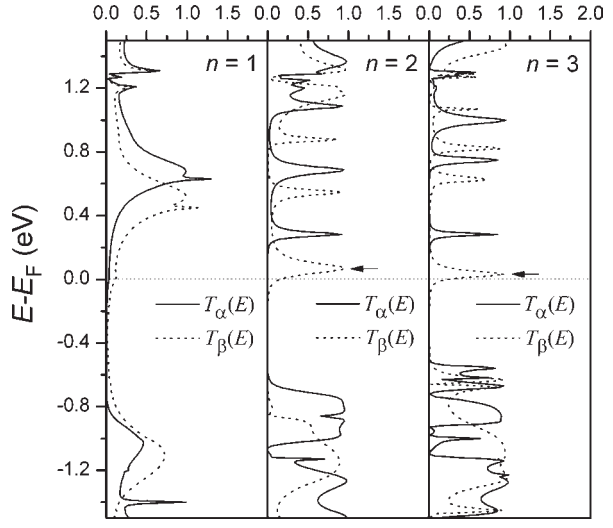

Figure 6. Spin-resolved transmission functions $T_\sigma(E)$ of Au−(α,γ)−Cr_n at zero bias voltage for n = 1, 2, and 3. The solid line represents the major spin (σ = α), and the dotted line represents the minor spin ($\sigma = \beta$).

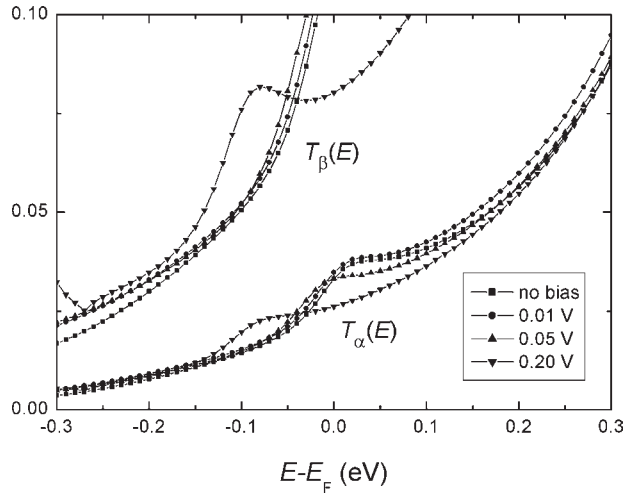

Figure 7. Enlarged transmission functions of Au−(α,γ)−Cr_1 at various bias voltages.

the antiferromagnetic state is semiconducting for both spins. The band gap of 0.29 eV can be attributed to occupation of the d_{xz} orbitals of both spins. In the ferromagnetic Cr−PA_∞, only the major spin conduction band is lifted up due to the interaction with the filled d_{xz} orbital having major spin electrons, but in the antiferromagnetic state, both conduction bands are destabilized through the interaction with the filled d_{xz} orbitals of both spins. This semiconducting feature allows us to design a spintronic device with Cr−PA_∞ despite the fact that only the ferromagnetic state is half-metallic.

Figure 6 shows the calculated transmission functions for Au−(α,γ)−Cr_n (n = 1, 2, 3) in their ferromagnetic state, and the conducting peaks are marked with arrows for n = 2 and 3. We can clearly see that the peaks from major and minor spins are separated. Above the Fermi energy, the minor spin peak is closer to the Fermi energy than the major one.[54] Below the Fermi

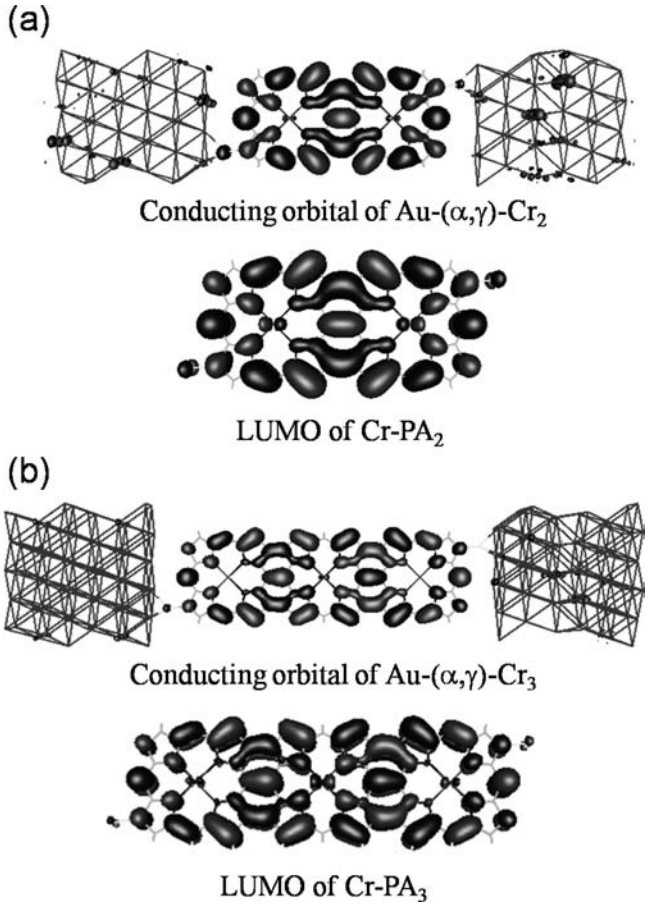

Figure 8. Comparison of the conducting orbital and the LUMO of the corresponding porphyrin array dithiol for (a) Au−(α,γ)−Cr_2 and (b) Au−(α,γ)−Cr_3.

energy, both are far away from the Fermi energy. This structure gives a spin-filtering effect to the device. To check bias effects on the transmission peaks, we performed calculations of electron transport at finite bias voltages with self-consistently converged electron density. The transmission function of Au−(α,γ)−Cr_1 changed little below the bias voltage of 0.2 V, as can be seen from Figure 7, and the transmission functions of Au−(α,γ)−$Cr_{2,3}$ presented in the Supporting Information show no considerable deformations but shifts of the peaks. Moreover, in the case of Au−(α,γ)−$Cr_{2,3}$, spin-polarized currents can be generated by an infinitesimally small bias voltage. Thus, we can safely assume that the spin-filtering effect remains intact upon application of a bias voltage. The spin polarization can be approximated by the ratio of T_α(E) and $T_\beta(E)$ at the Fermi energy. The spin polarization of Au−(α,γ)−Cr_1 is only about 59%, while those of Au−(α,γ)−$Cr_{2,3}$ are practically 100%, showing the half-metallic characteristics. While it might be difficult to form a very long ferromagnetic porphyrin array due to statistical effects, small oligomers can be made ferromagnetic because they are less prone to such effects. Therefore, it is a meaningful finding that Au−(α,γ)−Cr_n functions as a spin filter for an n as small as 2.

To understand the spin-filtering effect of Au−(α,γ)−$Cr_{2,3}$, we need to know where the peaks marked with arrows in Figure 6 come from. There are many possible channels through which the charge carriers can be conveyed. The molecular orbitals giving rise to the peaks are compared with the frontier orbitals of

dx.doi.org/10.1021/ja111565w |J. Am. Chem. Soc. 2011, 133, 9364–9369

Cr−$PA_{2,3}$ dithiols calculated with B3LYP/LanL2DZ using Gaussian 09. It turns out that the conducting molecular orbitals of Au−(α,γ)−$Cr_{2,3}$ match with the LUMOs of isolated Cr−$PA_{2,3}$ dithiols, respectively, as shown in Figure 8. Since the shapes of the orbitals in each pair are alike, the peaks represent the electron transport through LUMOs. The low conductance of Au−(α,γ)−Cr_1 comes from the fact that the LUMO level is located far away from the Fermi energy, while the high conductance of Au−(α,γ)−$Cr_{2,3}$ originates from the fact that the LUMOs are close to the Fermi energy. Applying the same argument for Cr−PA_∞, the porphyrin array is expected to have spin-filtering ability since its lowest unoccupied bands for α and β spins are about 0.30 eV apart.

It can be concluded from the above that the spin-dependent electron transport of Au−(α,γ)−Cr_n originates from the spin asymmetry of the electronic structure caused by the presence of a paramagnetic metal ion at the center of each porphyrin unit. This implies that the spin-filtering capacity is inherent in the Cr−PA_n, not in the interface. Therefore, Cr−PA_n's are expected to function as spin filters also for nonmagnetic electrodes such as carbon nanotubes or graphene nanoribbons that have a long spin coherence length.

We theoretically demonstrated that Cr−PA_n based on the one-dimensional porphyrin array containing paramagnetic Cr^{2+} ions is a new type of organometallic spin filter operating with a magnetic field. Its spin-filtering ability starts to appear from $n = 2$ for which its LUMO level becomes low enough to transport electrons from the electrode. For larger n's, it can be deduced from the band structures that Cr−PA_n will also function as a spin filter. The electrons are transported from one electrode to the lowest unoccupied levels of the minor spin electrons and then to the other electrode. Therefore, the spins of outgoing electrons are determined by the direction of magnetization of the Cr^{2+} ions, which can be controlled by an external magnetic field, since the calculated spin−orbit coupling effect is smaller than 0.005 eV (See Supporting Information). Though many others have proposed novel spintronic devices, none of them are realized due to the lack of a practical fabrication method at present. However, a spintronic device based on Cr−PA_n offers a synthesizable framework.

■ ASSOCIATED CONTENT

Supporting Information. Complete ref 50; discussion on the ferromagnetic-to-antiferromagnetic transition in Cr−PA_∞; assessment of the spin−orbit coupling effect in Cr−PA_∞; band structure of Cr−PA_∞ calculated using DFT+U methods; transmission functions of Au−(α,γ)−Cr_n, Fe_n, Co_n, Cu_n ($n = 1, 2, 3$); transmission functions of Au−(α,γ)−$Cr_{2,3}$ at finite voltages; discussion on the validity of the Landauer−Büttiker formula for the resonant tunneling regime; optimized geometries of Cr−PA_∞ and Au−(α,γ)−$Cr_{1,2,3}$. This material is available free of charge via the Internet at http://pubs.acs.org.

■ AUTHOR INFORMATION

Corresponding Author
kim@postech.ac.kr

■ ACKNOWLEDGMENT

This work was supported by the NRF (National Honor Scientist Program 2010-0020414, WCU R32-2008-000-10180-0) and KISTI (KCS-2008-K08-0002).

■ REFERENCES

(1) Aviram, A; Ratner, M. A. *Chem. Phys. Lett.* **1974**, *29*, 277–283.
(2) Cuniberti, G.; Fagas, G.; Richter, K. *Introducing Molecular Electronics*; Springer: Berlin and Heidelberg, 2005.
(3) Di Ventra, M. *Electrical Transport in Nanoscale Systems*; Cambridge University Press: Cambridge, 2008.
(4) Datta, S.; Das, B. *Appl. Phys. Lett.* **1990**, *56*, 665–667.
(5) Kim, W. Y.; Kim, K. S. *Acc. Chem. Res.* **2010**, *43*, 111–120.
(6) Herrmann, C.; Solomon, G. C.; Ratner, M. A. *J. Am. Chem. Soc.* **2010**, *132*, 3682–3684.
(7) Kim, W. Y.; Choi, Y. C.; Kim, K. S. *J. Mater. Chem.* **2008**, *18*, 510–4521.
(8) Kim, W. Y.; Choi, Y. C.; Min, S. K.; Cho, Y.; Kim, K. S. *Chem. Soc. Rev.* **2009**, *38*, 2319–2333.
(9) Wolf, S. A.; Awschalom, D. D.; Buhrman, R. A.; Daughton, J. A.; von Molnár, S.; Roukes, M. L.; Chtchelkanova, A. Y.; Treger, D. M. *Science* **2001**, *294*, 1488–1495.
(10) Lakshmi, S.; Roche, S.; Cuniberti, G. *Phys. Rev. B* **2009**, *80*, 193404.
(11) Ohno, H. *Science* **1998**, *281*, 951–956.
(12) Folk, J. A.; Potok, R. M.; Marcus, C. M.; Umansky, V. *Science* **2003**, *299*, 679–682.
(13) Park, J. H.; Vescovo, E.; Kim, H. J.; Kwon, C.; Ramesh, R.; Venkatesan, T. *Nature* **1998**, *392*, 794–796.
(14) Hwang, H. Y.; Cheong, S. W. *Science* **1997**, *278*, 1607–1609.
(15) Tsukagoshi, K.; Alphenaar, B. W.; Ago, H. *Nature* **1999**, *401*, 572–574.
(16) Kikkawa, J. M.; Awschalom, D. D. *Nature* **1999**, *397*, 139–141.
(17) Sanvito, S. *J. Mater. Chem.* **2007**, *17*, 4455–4459.
(18) Lee, E. C.; Choi, Y. C.; Kim, W. Y.; Singh, N. J.; Lee, S.; Shim, J. H.; Kim, K. S. *Chem.—Eur. J.* **2010**, *16*, 12141–12146.
(19) Son, Y.; Cohen, M. L.; Louie, S. G. *Nature* **2006**, *444*, 347–349.
(20) Luo, P.; Lee, J. Y. *J. Phys. Chem. C* **2009**, *113*, 12637–12640.
(21) Dutta, S.; Manna, A. K.; Pati, S. K. *Phys. Rev. Lett.* **2009**, *102*, 096601.
(22) Martins, T. B.; da Silva, A. J. R.; Miwa, R. H.; Fazzio, A. *Nano Lett.* **2008**, *8*, 2293–2298.
(23) Son, Y. W.; Cohen, M. L.; Louie, S. G. *Phys. Rev. Lett.* **2006**, *97*, 216803.
(24) Hod, O.; Barone, V.; Peralta, J. E.; Scuseria, G. E. *Nano Lett.* **2007**, *7*, 2295–2299.
(25) Maslyuk, V. V.; Bagrets, A.; Meded, V.; Arnold, A.; Evers, F.; Brandbyge, M.; Bredow, T.; Mertig, I. *Phys. Rev. Lett.* **2006**, *97*, 097201.
(26) Wang, L.; Cai, Z.; Wang, J.; Lu, J.; Luo, G.; Lai, L; Zhou, J.; Qin, R.; Gao, Z.; Yu, D.; Li, G.; Mei, W. N.; Sanvito, S. *Nano Lett.* **2008**, *8*, 3640–3644.
(27) Zhang, Z.; Wu, X.; Guo, W.; Zeng, X. C. *J. Am. Chem. Soc.* **2010**, *132*, 10215–10217.
(28) Zhou, L.; Yang, S.; Ng, M.; Sullivan, M. B.; Tan, V. B. C.; Shen, L. *J. Am. Chem. Soc.* **2008**, *130*, 4023–4027.
(29) Wu, X.; Zeng, X. C. *J. Am. Chem. Soc.* **2009**, *131*, 14246–14248.
(30) Diefenbach, M.; Kim, K. S. *Angew. Chem., Int. Ed.* **2007**, *46*, 7640–7643.
(31) Kang, B. K.; Aratani, N.; Lim, J. K.; Kim, D.; Osuka, A.; Yoo, K. *Chem. Phys. Lett.* **2005**, *412*, 303–306.
(32) Tagami, K.; Tsukada, M.; Matsumoto, T.; Kawai, T. *Phys. Rev. B.* **2003**, *67*, 245324.
(33) Long, M.; Chen, K.; Wang, L.; Qing, W.; Zou, B. S.; Shuai, Z. *Appl. Phys. Lett.* **2008**, *92*, 243303.
(34) Ribeiro, F. J.; Lu, W. C.; Bernholc, J. *ACS Nano* **2008**, *2*, 1517–1522.
(35) Holten, D.; Bocian, D. F.; Lindsey, J. S. *Acc. Chem. Res.* **2002**, *35*, 57–69.
(36) Yamaguchi, Y. *J. Chem. Phys.* **2002**, *117*, 9688–9694.
(37) Chen, Y.; Prociuk, A.; Perrine, T.; Dunietz, B. D. *Phys. Rev. B* **2006**, *74*, 245320.
(38) Tsuda, A.; Osuka, A. *Science* **2001**, *293*, 79–82.
(39) Reed, C. A.; Kouba, J. K.; Grimes, C. J.; Cheung, S. K. *Inorg. Chem.* **1978**, *17*, 2666–2670.

(40) Collman, J. P.; Hoard, J. L.; Kim, N.; Lang, G.; Reed, C. A. *J. Am. Chem. Soc.* **1975**, *97*, 2676–2681.
(41) Wang, X.; Gray, S. D.; Chen, J.; Woo, L. K. *Inorg. Chem.* **1998**, *37*, 5–9.
(42) Aratani, N.; Osuka, A.; Kim, Y. H.; Jeong, D. H.; Kim, D. *Angew. Chem., Int. Ed.* **2000**, *39*, 1458–1462.
(43) Kim, W. Y.; Kim, K. S. *J. Comput. Chem.* **2008**, *29*, 1073–1083.
(44) Kim, W. Y.; Kim, K. S. *Nat. Nanotechnol.* **2008**, *3*, 408–412.
(45) Min, S. K.; Kim, W. Y. Kim; Cho, Y.; Kim, K. S. *Nat. Nanotechnol.* **2011**, *6*, 162–165.
(46) Kresse, G.; Furthmüller, J. *Phys. Rev. B* **1996**, *54*, 11169.
(47) Perdew, J. P.; Burke, K.; Ernzerhof, M. *Phys. Rev. Lett.* **1996**, *77*, 3865–3868.
(48) Kresse, G.; Joubert, D. *Phys. Rev. B* **1999**, *59*, 1758–1775.
(49) Soler, J. M.; Artacho, E.; Gale, J. D.; García, A.; Junquera, J.; Ordej, P.; Sanchez-Portal, D. *J. Phys.: Condens. Matter* **2002**, *14*, 2745–2779.
(50) Frisch, M. J. et al. *Gaussian 09*, Revision A.1; Gaussian, Inc.: Wallingford CT, 2009.
(51) Liao, M.; Scheiner, S. *J. Chem. Phys.* **2002**, *117*, 205–219.
(52) Youn, S. J.; Sahu, B. R.; Kim, K. S. *Phys. Rev. B.* **2002**, *65*, 052415.
(53) Rohrbach, A.; Hafner, J.; Kresse, G. *Phys. Rev. B* **2004**, *69*, 075413.
(54) The sharp resonance transmission peak near the Fermi energy may entail non-negligible interactions of a charge carrier with other electrons or phonons due to its finite traverse time, which cannot be captured by a single-particle picture such as the Landuer−Büttiker formula. However, the formula is still valid in a low-bias and low-temperature limit if the couplings between a molecule and electrodes like our case are sufficiently strong so that electron transfer is occurred within a very short time. More details are discussed in the Supporting Information.